Broadband optical coupling between microstructured fibers and photonic band gap circuits: Two-dimensional paradigms

James Bauer and Sajeev John
Department of Physics, University of Toronto, 60 Saint George Street, Toronto, ON, M5S 1A7, Canada
(Received 6 June 2007; published 18 January 2008)

We demonstrate high efficiency, broadband coupling between photonic crystal waveguides and photonic crystal fibers (PCFs) using simple two-dimensional design models. We demonstrate an effective large-bandwidth small-footprint beam collimator for light exiting a two-dimensional subwavelength scale photonic crystal waveguide consisting of an air core. This collimator relies on destructive interference between diffracted light from the mouth of the waveguide and the light emitted by surface resonators. We demonstrate efficient coupling between air-core photonic crystal waveguides and various two-dimensional models of photonic crystal fibers. A hollow-core photonic crystal fiber, described by an air defect with a Bragg stack cladding on either side, yields a coupling efficiency of better than 94% over a bandwidth of 25% of the center frequency, with peak transmittance exceeding 98%. A small-mode-area PCF, consisting of a subwavelength solid core attached by spokes to the PCF cladding, is modeled by a slab waveguide. In this latter case, we demonstrate coupling efficiency better than 94% over a bandwidth of 17%, with peak transmittance exceeding 99%. Combining collimation at the photonic crystal exit port and a nonadiabatic taper in a small-mode-area PCF, we obtain over 98% coupling efficiency over a bandwidth of 135 nm centered at a wavelength of 1.5 μm. These results provide valuable paradigms for efficient transfer of optical information between photonic band gap (PBG) microcircuits and PCF-enabled telecommunication networks.

DOI: 10.1103/PhysRevA.77.013819 PACS number(s): 42.70.Qs, 42.79.Ag, 42.79.Gn

I. INTRODUCTION

Photonic band gap (PBG) materials [1,2] are a special class of photonic crystals that offer a robust platform for integrated optics. Unlike conventional paradigms such as silicon on insulator (SOI) waveguides that guide light on a chip by total internal reflection (index guiding), PBG-based microcircuits can guide light in air-core waveguides by an interference (light localization [3]) mechanism. The PBG-based optical microchip can guide light in a three-dimensional (3D) network, over a broadband of wavelength channels. By virtue of the photonic band gap, guided light cannot diffract or scatter out of the circuit path even near sharp waveguide bends or other subwavelength apertures. Various desirable signal processing and carrying devices have been theoretically proposed in two dimensions, including waveguides [4], add-drop filters [5], and sharp waveguide bends [6]. Experimental implementation of these designs, however, require 2D membranes that confine light by total internal reflection in the third dimension (normal to the plane of the 2D chip). Consequently, scattering loss into the third dimension occurs whenever in-plane discrete translational symmetry is broken. One alternative platform for implementing such devices in 3D, without radiation loss, is through PBG heterostructures [7–10]. These structures have a 2D photonic crystal (PC) layer sandwiched above and below by a 3D PBG material. The heterostructure possesses a full 3D PBG and the intercalated 2D microchip layer allows embedding of previous 2D designs in a three-dimensional setting, without out-of-plane scattering loss. Since the waveguide size in these structures is less than the free space wavelength of light, lossless coupling between PBG microcircuits and optical fiber networks presents an important challenge. In passing from the Cartesian geometry and small mode cross section of the PBG microchip to the cylindrical geometry and large mode cross section of an optical fiber, optical scattering losses can be significant. In this paper, we present two-dimensional paradigms for realizing low-loss broadband coupling between the fiber and optical microchip using "small footprint" microstructures.

Previous attempts at coupling light into PC waveguides from external sources can be broadly classified into four different categories. The first is adiabatic coupling, where the waveguide is slowly changed over many lattice constants [11–15]. These designs predict near 100% transmission provided the change is slow (adiabatic). The resulting designs are also relatively insensitive on the frequency of the light. Conversely these designs require very small changes over relatively large length scales making manufacturing tolerances very strict. The slow structural change over many lattice constants also means that these couplers have relatively large footprints, on the order of tens to hundreds of PC unit cells. A second approach to the coupling problem relies on transferring light to high-index PC waveguides from high-index "slab" waveguides [16–24]. The slab waveguide consists of a high dielectric core (usually the same high-index material as the PC waveguide core) surrounded by a lower index cladding. Here, light is contained by total internal reflection. The coupling between these two types of waveguides can be quite high (97% [18]) due to the similarity between the two waveguide structures. Nevertheless, they are restricted to PC waveguides that have a high-index solid core. Moreover, the problem of coupling light to an optical fiber still remains. Adiabatic taper of the slab waveguide to match the impedance of the optical fiber leads once again to a large footprint coupling device. To circumvent this problem, vertical grating couplers that diffract light into the normal direction from the photonic chip to an optical fiber have

been proposed and implemented [25–31]. The third approach considers coupling into low-index core PBG waveguides. When coupling into these waveguides (where light is confined by the localization effect of a PBG) from conventional waveguides, various PC "horns" [32–36] have been proposed. These horns are characterized by sharp tapers which structurally resemble a funnel. The funnel is constructed by removing PBG material such that the small end of the taper matches a single-mode PBG waveguide, whereas the large end matches a much larger slab waveguide. These designs fall outside the adiabatic regime and generally are more sensitive on the frequency of the light. The best reported peak coupling efficiency within this approach is 93.5% [36], found by a genetic algorithm. This optimum result was obtained for a single frequency, without consideration for the coupling bandwidth. These "horns" require a moderate footprint and generally occupy an area of about forty unit cells. The fourth strategy involves coupling into PC "membrane" waveguides using tapered optical fibers [37–43]. The fiber is tapered to a small diameter such that the guided mode has a substantial portion of its energy in the evanescent field outside the fiber core. The fiber is then brought near and parallel to the PC membrane waveguide and the field resonantly couples through the evanescent field into the PC waveguide mode. Using this method, coupling efficiencies of 95% can be realized over a bandwidth of 1.3% [41]. This method is suitable for coupling to "membrane" PBG waveguides, but is not practical for PBG air waveguides which require a PBG material cladding. The narrow bandwidth of this method is limited to the frequency ranges where the membrane and fiber guided modes have comparable momentum components along the waveguiding axis.

In this paper, we exploit the design flexibility provided by microstructured optical fibers to provide broadband impedance matching to air-waveguide circuits in 3D PBG microcircuits. It is assumed that adiabatic modification of fiber microstructure along the length of the fiber can be readily achieved to seamlessly couple light to a conventional long-haul telecommunications fiber. PC (or "holey") fibers are microstructured dielectric fibers, composed of a two dimensional (usually) periodic array of two dielectric materials that run the length of the fiber. The effect of the periodic array is to introduce forbidden regions in frequency and propagation wave-vector $(a/\lambda, k_z a)$ space, where modes do not exist. A guided mode can be created by introducing a defect in the periodic array that inserts a mode in this forbidden band gap. Various desirable properties can be engineered in such structures, including dispersion management [44,45], "endlessly single mode" behavior [46], and even guiding light in the low index material [47] (not possible using total-internal reflection guiding). Another important feature that can be engineered is the field mode profile. Specialty small-mode-area fibers [48], highly birefringent fibers [49], and polarization maintaining fibers [50] are some of the engineering possibilities in PC fibers. If 2D–3D PC heterostructures (or any other small mode area PBG waveguides) are to be practical, then the ability to efficiently couple light in and out of these waveguides over a suitable bandwidth is crucial. In this paper, we demonstrate that recently introduced PC fibers provide this capability.

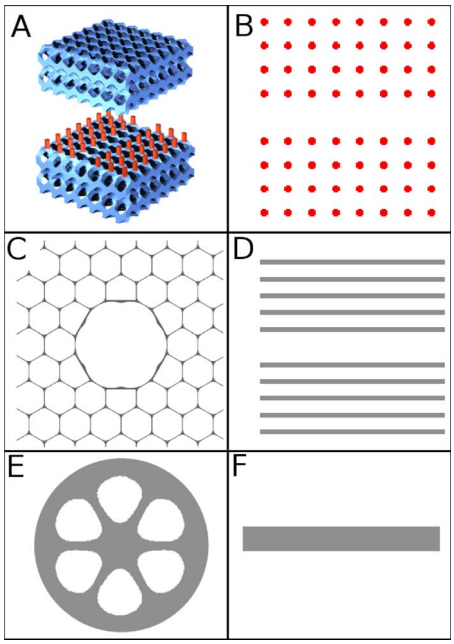

FIG. 1. (Color online) (a) Depicted is an air waveguide in a 2D–3D PBG heterostructure, consisting of a 2D lattice of square rods sandwiched between two 3D PBG materials above and below. A single-mode waveguide is created by removing a row of rods in the 2D layer. (b) The 2D model of the waveguide from (a) is a 2D lattice of dielectric rods with a missing row. (c) A cross section of a hollow-core PBG fiber. The large central (air) defect supports a guided mode (sometimes multiple modes) that is radially contained by the PBG effect. This structure is invariant along the fiber axis. (d) depicts our 2D model of the fiber in (c). This fiber Bragg waveguide, similar to its 3D counterpart, contains light primarily in the air defect, confined through wave interference rather than total internal reflection. (e) A schematic of a small-mode-area fiber where a dielectric island is supported by thin dielectric veins. This fiber is modeled in two dimensions as a dielectric slab (f).

There are two possibilities if PC fibers are used: hollow-core PC fibers or small-mode-area solid core PC fibers. In the latter, a large hollow core is typically impregnated with a small solid core suspended by thin spokes that traverse the length of the fiber. In this paper we study dimensionally reduced versions of these fibers. The two-dimensional analog of a hollow-core PC fiber (PCF) is a low-index defect within a periodic one-dimensional structure (an air defect in a Bragg stack cladding, referred to as a Bragg waveguide). The analogue of the small-mode-area fibers is a thin dielectric slab surrounded by air (we neglect the thin spokes that connect the small area core to the PCF cladding). Figure 1 depicts the correspondences between physical 3D systems and our model 2D systems. A 3D PBG heterostructure microcircuit is shown in Fig. 1(a), along with an example of a hollow-core PBG fiber [Fig. 1(c)] and a small-mode-area PBG fiber [Fig. 1(e)]. The 2D models of these three waveguides, which will be discussed in greater detail in the body of the paper, are schematically depicted in Fig. 1(b) for the PBG heterostructure, Fig. 1(d) for the hollow-core PBG fiber, and finally Fig.

1(f) for the small-mode-area fiber. In a realistic 2D–3D PBG heterostructure, air waveguides can be designed to have predominantly TM polarization [7–10] [Fig. 1(e)—field aligned with the rods in the two-dimensional layer]. Accordingly, in our 2D paradigm, we choose the TM modes in a 2D square lattice of dielectric rods embedded in air. The design of small-footprint couplers for low-index PC waveguides (light contained by the PBG effect) presents a unique opportunity for a large-bandwidth efficient coupler.

This paper is organized as follows. Section II describes the PC waveguide termination properties relevant to the coupling calculations that follow. In particular we delineate the nature of the optical diffraction at the PC surface and we introduce a broadband beam collimator. Section III introduces the Bragg fiber waveguide (the dimensionally reduced hollow core PC fiber) and some of its properties. We then study coupling between the model fiber and PC waveguides, with and without the collimation architecture. Section IV discusses the slab waveguide (the dimensionally reduced small-mode-area PC fiber) and its coupling to the PC waveguide. The ability of this slab waveguide to influence the reflection spectrum is examined and a nonadiabatic taper is used to optimize coupling efficiency. Section V summarizes the key results of this paper.

II. SURFACE DIFFRACTION AND BEAMING FROM A PBG AIR WAVEGUIDE

The natural dimensional reduction from a 2D–3D PBG heterostructure air-waveguide exit port is to consider the surface termination of an air waveguide in a 2D square lattice of dielectric rods embedded in air. Consider a square lattice of dielectric rods of radius $r=0.15a$ where a is the lattice constant of the PC with dielectric constant $\epsilon_{rod}=11.9$ embedded in a background of $\epsilon_{background}=1.0$. This structure has a 2D PBG for the TM modes between $a/\lambda=0.330$ and $a/\lambda=0.475$ (where λ is the free-space wavelength). A single mode waveguide is created by removing one row of rods. This mode spans the frequency range of the band gap. We focus on the normalized frequency range between $a/\lambda=0.35-0.45$.

Normally, light exiting from an aperture that is approximately the size of the wavelength of light, diffracts sharply into free space [51]. Here, we define the surface of the PC by cleaving it between rows of silicon rods. This ensures that there are no surface modes in the frequency range of interest [52]. We use the finite-difference-time-domain method with perfectly matched layer boundary conditions [60] with spatial resolution $\delta x=0.0625a$ and time resolution $c\delta t=0.025a$ for all calculations in this study. Reflectance (and in later sections, transmittance) spectra are determined by measuring the Fourier-transformed Poynting vector through a line $50a$ from the exit port. Figure 2 shows the structure and snapshots of the steady-state electric field intensity $|\mathbf{E}|^2$ for frequencies $a/\lambda=0.365$, 0.375, 0.385, 0.395, 0.405, 0.415, 0.425, and 0.435. We see that the field exiting the PC waveguide diffracts sharply, since its mouth width is nearly the free-space wavelength of the light. The curve shows the reflection spectrum, which is below 10% for all frequencies plotted.

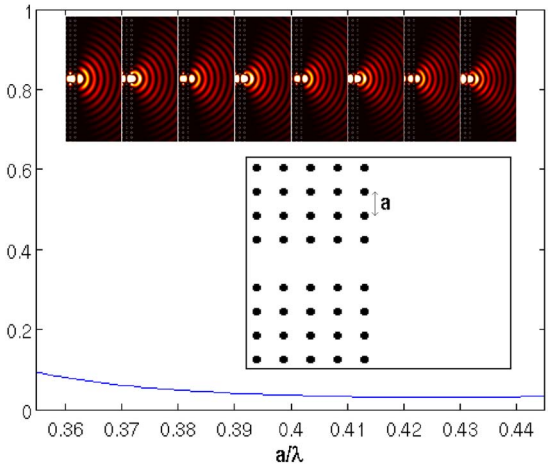

FIG. 2. (Color online) Snapshots of the electric field intensity for light diffracting from a PBG air waveguide into free space for normalized frequencies (from left to right) $a/\lambda=(0.365, 0.375, 0.385, 0.395, 0.405, 0.415, 0.425,$ and $0.435)$. The curve is the reflectance back into the waveguide vs normalized frequency a/λ. The inset shows the junction of the air waveguide and free space. The structural parameters are rod radius $r=0.15a$, $\epsilon_{rod}=11.9$, and $\epsilon_{background}=1.0$, where a is the lattice constant of the PBG structure. Light exiting the air waveguide diffracts sharply into free space.

Previous studies have reported that the far-field radiation pattern of light exiting a small aperture can be modified with appropriate modification of the terminating surface. In particular, modifying the surface structure near the waveguide mouth to introduce the appropriate (lossy) surface modes yields a very collimated beam for specific frequencies [53–58]. However, this collimation is very sensitive to the frequency of the light. In practice, collimation occurs only over a bandwidth of 6% [55] of the center waveguide frequency. Since the bandwidth of the PC waveguide is 25% of the center frequency, a more broadband collimation mechanism is highly desirable.

In order to achieve broadband collimation from the PC air-waveguide exit port, we utilize an alternative paradigm. Consider a linear, nondispersive dielectric slab of thickness t surrounded by vacuum. Plane waves incident on this structure at normal incidence will exhibit a series of transmission resonances related to the multiples of half wavelengths of light fitting within the dielectric slab. One property of the transmitted wave is that it exhibits a π phase shift as its frequency is swept through a resonance. In the context of our PC air waveguide, there are multiple channels (transmission angles) excited as a result of wave diffraction from the small-aperture waveguide mouth. A π phase shift of the wavefield from a secondary source, placed near the waveguide mouth and excited by light from the waveguide itself, can be used to cancel certain diffraction angles through destructive interference with the wavefield from the primary source (the waveguide itself). By introducing larger rods on either side of the waveguide exit, that support a lossy resonance mode in the working frequency range, the far-field radiation can be strongly modified.

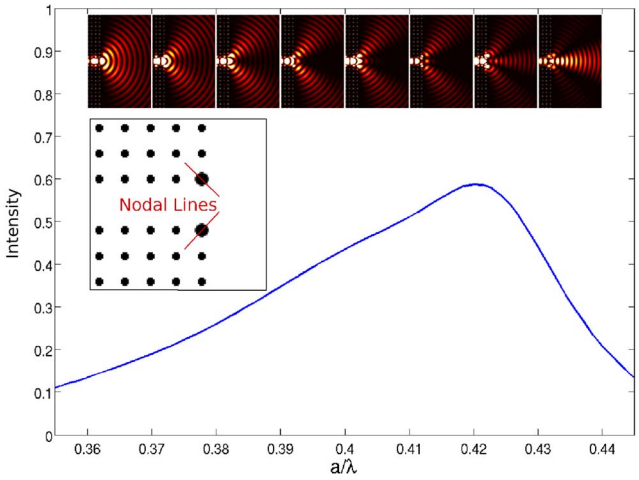

FIG. 3. (Color online) Snapshots of the electric field intensity for light exiting the PBG air waveguide with larger rods (resonators) at the waveguide exit port to free space, for normalized frequencies (from left to right) $a/\lambda=(0.365,0.375,0.385,0.395,0.405,0.415,0.425,$ and $0.435)$. The curve shows the reflectance spectrum, with peak reflection at $a/\lambda=0.42$. The structure is shown in the inset. The larger rods at the waveguide exit have radius $r_{exit}=0.26a$. The other structural parameters are identical with those in Fig. 2. The nodal lines of the lossy resonance mode supported by the large exit rods are shown. On resonance ($a/\lambda=0.42$) there is considerable back reflection into the waveguide. Above resonance, beam collimation appears.

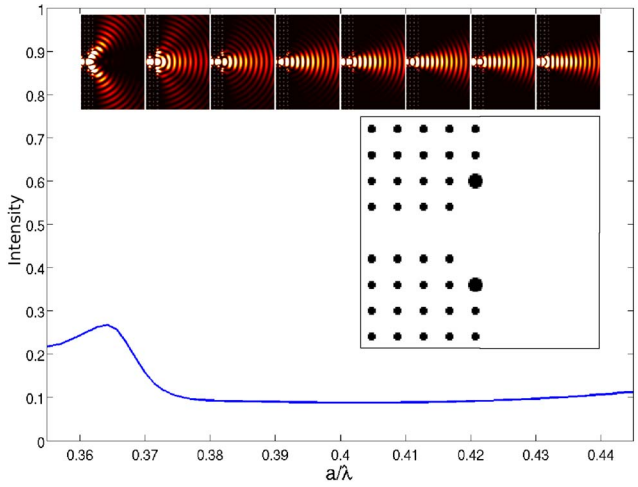

FIG. 4. (Color online) PBG exit-port beam collimator. The position of the modified exit rods (resonators) have been moved to the second nearest neighbor and increased in size ($r_{exit}=0.275a$), and the first nearest neighbor rods at the exit have been removed (see inset). This reduces back reflection into the waveguide. The curve shows the reflectance back into the PC waveguide, which is less than in Fig. 3. Snapshots of the electric field intensity at frequencies (from left to right) $a/\lambda=(0.365,0.375,0.385,0.395,0.405,0.415,0.425,$ and $0.435)$ are also shown. Beam collimation is achieved over a broad range of frequencies above the resonance $a/\lambda=0.37$. This arises from destructive interference between the standard diffraction pattern from the waveguide-exit port and the π shifted light from the resonators in the off-axis direction. The resonance frequency may be tuned by changing the size of the modified exit rods.

Figure 3 depicts a modified waveguide exit port in which the two dielectric rods closest to the waveguide termination have been replaced by larger rods of radius $r_{exit}=0.26a$. These larger rods act as secondary sources of light exiting the air waveguide. Figure 3 shows the reflection spectrum and snapshots of the electric intensity at frequencies $a/\lambda=0.365$, 0.375, 0.385, 0.395, 0.405, 0.415, 0.425, and 0.435. The reflection spectrum shows a resonance with peak near $a/\lambda=0.42$. Far below resonance ($a/\lambda=0.365$) the electric field intensity is nearly identical to the unmodified case. As the frequency approaches the resonance, the electric field intensity below resonance has most of the field energy symmetrically exiting the waveguide at approximately 50° from the waveguide direction (the normal direction). The far-field radiation pattern above resonance shows markedly different behavior: the field remains collimated with very little field propagating at far-from-normal directions (PC beaming). The difference can be attributed to the interference between the two possible paths the light may take. The first path (path 1) the light may take is simply to exit the waveguide, bypassing the resonators (as is the case far from resonance at $a/\lambda=0.365$. Light taking this path will sharply diffract roughly uniformly over 180°, as in the case without any surface modifications. The second path (path 2) is through the resonators. The resonators support a dipole like (lossy) mode with nodal line as shown in the Fig. 3. When the frequency is below resonance, light that takes path 2 is in-phase with light that takes path 1 in the off-normal direction, and out-of-phase in the normal direction. This is evident from the electric field intensity snapshots below resonance, as seen in Fig. 3. As the frequency is swept through and above the resonant frequency, the light that takes path 2 undergoes a π phase shift and the far-field radiation pattern switches to the reverse behavior. Constructive interference occurs in the normal direction, and destructive interference occurs at off-normal directions, leading to a collimated beam.

While the output port architecture in Fig. 3 illustrates the collimation principle, it is highly desirable for broadband fiber-to-chip coupling for the beam to remain collimated over a larger range of frequencies and for reflection at the port to be minimized. The first requirement can be met by adjusting the size of the defect rods to lower the resonant frequency. The second requirement is met by moving the defect rods one unit cell away, to reduce scattering from the secondary sources back in into the waveguide.

Figure 4 shows an improved structure that exhibits this beaming phenomenon. Reflection is now reduced, and the collimated beam persists for a very large bandwidth (17.5% of the center frequency), much larger than the narrow working range of previous designs based on lossy surface modes [53–58]. Our design is also insensitive to the exact resonant frequency of the large rods, but relies instead on being *above* their resonant frequency. Consequently, this design is robust to some amount of manufacturing error. We note, however, that the back reflection is slightly lower when there are no surface modifications. Our physically motivated design for beam collimation is consistent with other approaches based

on genetic algorithms [59]. Our approach optimizes collimation over a broad band of frequencies rather than focusing on a single frequency. The following sections examine the utility of various photonic crystal fiber designs in combination with exit port modification (beam collimation) to achieve the highest quality broadband coupling to and from a PBG circuit.

III. PBG CHIP TO HOLLOW CORE PBG FIBER COUPLING

A. Bragg waveguide model for PBG fibers

The two-dimensional analog of a hollow-core PBG fiber is a low-index (air) defect core sandwiched above and below by one-dimensional Bragg stacks (Bragg waveguide). The indices of refraction ($n_i=\sqrt{\epsilon_i}$) of the two cladding regions are chosen to consist of alternating layers of index $n_1=1.5-1.8$ and index $n_2=1.0$. Waveguide modes occur because the enlarged core (defect) of index n_2 confines a fundamental even mode within the one-dimensional band gap of the surrounding cladding. These states are localized in the low index core through wave interference rather than total internal reflection. These modes are only localized in the direction perpendicular to the "fiber" axis but are free to propagate along the axis (the fields have a z dependence of $e^{ik_z z}$).

Enlarging one air region in an otherwise perfect Bragg stack creates a ladder of localized defect modes at different frequencies for each choice of axis propagation wave-vector k_z. Unlike the ladder of defect modes in a quantum mechanical potential well, some of the defect modes of the PBG fiber will be contained within the band gaps of the Bragg stack cladding (guided modes), whereas some will fall outside these band gaps (lossy modes). We restrict our choices of hollow fiber core width so that there is only one fundamental even-parity mode within the bandwidth of the PC waveguide mode. This reduces the problem of coupling to that between single-mode waveguides on either side of the junction. If higher-order even modes exist in the fiber, they will also couple with the even mode exiting the PC waveguide. Such extraneous modes provide another mechanism for coupling loss. The odd modes are ignored in this analysis since the even PC waveguide mode will not couple to these modes by symmetry.

Figure 5 shows an example of a 2D hollow core PBG fiber Bragg waveguide dispersion relation. There is one fundamental even guided mode between the first and second cladding bands, and a higher-order even mode between the second and third cladding bands. The odd modes have not been plotted. The dispersion relation (expressed as a transcendental equation) is obtained analytically from Maxwell's equations. This equation is solved numerically for the guided mode dispersion and plotted along with the projected band structure of the fiber cladding (Bragg stack). We make the following observations about the 2D PBG hollow core fiber model: Increasing the index of refraction of the cladding layers tends to lower the frequency of the cladding modes. Similarly, increasing the width of the higher-index cladding layers also lowers the frequency of the cladding modes. Increasing the defect (fiber core) width tends to lower the frequency of the core guided modes and decreases the frequency spacing between the rungs in the ladder of guided modes. This behavior is analogous to that of bound states in a quantum mechanical potential well as the width of the potential well is increased.

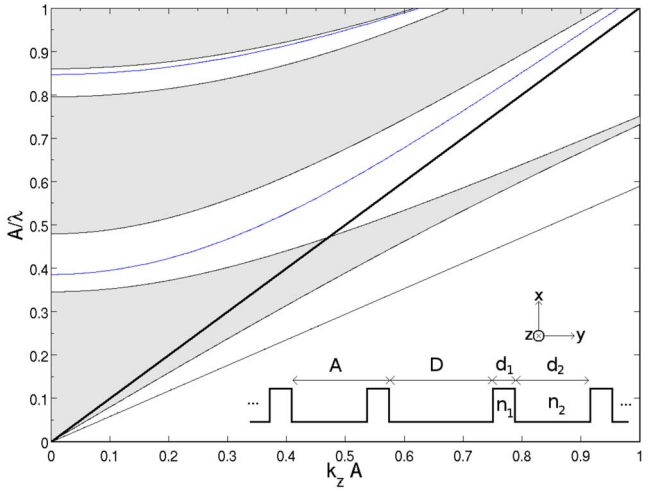

FIG. 5. (Color online) A dispersion relation of the TM modes (**E** polarized in the x direction, as shown in the inset diagram) of a Bragg waveguide (hollow core PBG fiber) with $d_1=0.3A$, $d_2=0.7A$, $n_1=1.7$, $n_2=1.0$, and $D=1.3A$ where A is the lattice constant of the PBG cladding layers. The horizontal axis is the normalized propagation constant k_zA and the vertical axis is the normalized frequency A/λ. The gray regions are the projected bands of the cladding and the white regions indicate the photonic band gaps. The lower (blue) dotted curve is the lowest-order guided even mode, and the upper (blue) curve is a higher-order guided even mode. The odd modes have been omitted from this diagram. The solid straight (black) lines are the n_1 and n_2 light lines. A diagram of the refractive index profile is shown in the bottom right.

B. PC air waveguide to hollow core fiber coupling

In this section we study end coupling between unmodified PC air waveguides and two-dimensional hollow-core PBG fiber Bragg waveguides. We use the finite difference time domain method to calculate the reflectance and transmittance spectra for a family of different 2D fiber models. The fiber (Bragg waveguide) parameter space includes a variation in the defect width D between $1.2A$ and $2.1A$ (where A is the Bragg stack cladding lattice constant), a variation in the index of refraction of the high-index cladding component layer n_1 between 1.5 and 1.8, and a variation of the lattice constant ratios A/a between the PC waveguide and the fiber cladding (Bragg stack) from $A/a=1.2$ to 2.0. The 2D hollow core fiber is placed immediately adjacent to the last row of rods of the PC and a Gaussian pulse that covers the PC waveguide bandwidth is excited in the PC waveguide at a distance of approximately $60a$ from the PC exit port. The reflectance (transmittance) spectra are determined by measuring the Fourier-transformed Poynting vector through a line $50a$ before (after) the PC-to-fiber junction.

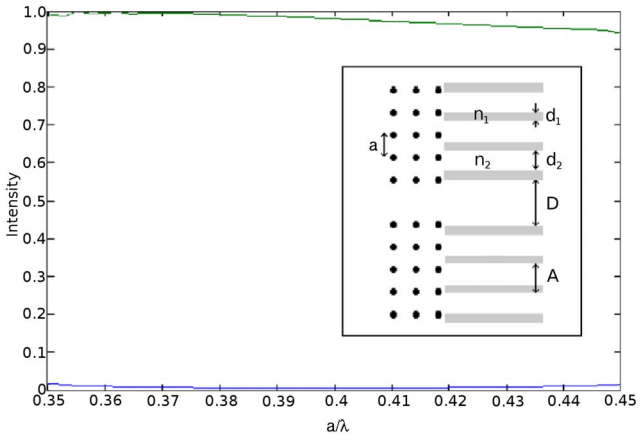

FIG. 6. (Color online) The transmittance (upper curve) and reflectance (lower curve) for light coupling from the PBG air waveguide to the hollow core PBG fiber. The PBG air-waveguide parameters are $\epsilon_{rod}=11.9$, $\epsilon_{background}=1.0$, and $r=0.15a$, where a is the PC lattice constant. The hollow core fiber has $D=1.6A$, $d_1=0.3A$, $d_2=0.7A$, with refractive indices $n_1=1.8$, $n_2=1.0$, where A is the fiber cladding lattice constant. The two lattice constants are related by $A/a=1.3$.

Figure 6 shows the reflectance and transmittance spectra for the structure with the highest transmittance within the parameter space. The reflectance is below 2% and the transmittance is better than 94% from $a/\lambda=0.35$ to $a/\lambda=0.45$. To study the influence of the fiber core width on coupling we calculate the reflectance and transmittance for various core widths. Figure 7 shows the results when the fiber core width D is changed from this optimum value, the transmittance still remains above (82%) throughout the range $D=1.2A$ to $D=2.1A$ (or in units of the PC lattice constant, $D=1.56a$ to $D=2.73a$), dropping near the extremes. The back reflection into the PC waveguide when coupled to the fiber is lower than if PC waveguide simply diffracts or beams light to free space. This suggests that the fiber to PC waveguide junction provide better impedance matching than the PC waveguide to air interface. The large range of D values suggests some flexibility in possible coupling designs. Nevertheless, the PBG fiber cladding plays an important role in capturing the light exiting the PC waveguide. Since we are restricting both waveguides to be single-mode (even parity), the transmission and reflection spectra are the same whether coupling from PC air waveguide to fiber or from fiber to PC air waveguide. This was verified by numerical simulation.

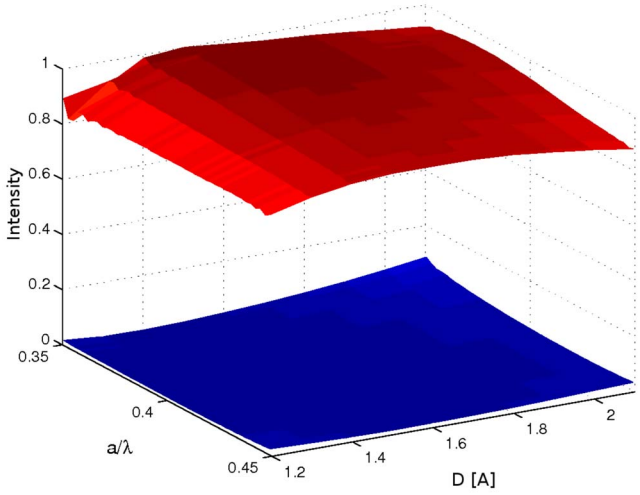

FIG. 7. (Color online) The transmittance (upper surface) and reflectance (lower surface) for coupling from a PBG air waveguide to a hollow core PBG fiber (see Fig. 6) as a function of both frequency a/λ and fiber core diameter D (in units fiber cladding lattice constant A). Here the fiber parameters are $d_1=0.3A$, $d_2=0.7A$, $n_1=1.8$, $n_2=1.0$, and the PC air-waveguide parameters are $\epsilon_{rod}=11.9$, $\epsilon_{background}=1.0$, and $r=0.15a$.

Changing the fiber cladding refractive index, n_1, changes the frequency of the cladding modes, but has a relatively small effect on the guided mode frequency and its mode profile. Figure 8(a) shows the transmittance and reflectance as a function of a/λ and n_1 with the optimum fiber core diameter $D=1.6A$. The transmittance shows little variation with frequency, but drops to approximately 80% at $n_1=1.5$, while the reflectance remains constant. This can be explained by looking at the Bragg waveguide dispersion relation for the two extreme cases: At $n_1=1.5$ the lowest cladding band is close to the guided core mode [see Fig. 8(b)]. A snapshot of the steady-state electric field intensity at $a/\lambda=0.4$ [Fig. 8(c)] reveals optical losses through the cladding due to proximity of the continuum of cladding modes. Figure 8(d) shows the dispersion relation of the Bragg waveguide with $n_1=1.8$. The lossy cladding modes are now further away in frequency from the guided mode. As a result, the electric field intensity in the fiber cladding is negligible [Fig. 8(e)].

To summarize, the transmittance from an unmodified PC air waveguide to a 2D model hollow-core PBG fiber is better than 94% efficient over a bandwidth of 25% of the center frequency, with less than 2% back reflection. The peak transmittance is 98%. The coupling is also tolerant to Bragg waveguide (fiber core) width changes, with transmittance above 90% for a range of $D=1.4A$ to $D=2.0A$ over the entire frequency range. The results are more sensitive on the index of refraction of the high index layers in the hollow core PBG fiber cladding, with higher values of the index minimizing the effect of loss through the cladding modes.

C. Beaming from PC air waveguide to hollow core fiber

In this section we study the role of the collimation effects in high-efficiency PC waveguide to fiber coupling. In particular, we consider the robustness of coupling to design variation provided by an exit-port beam collimator. We calculate the reflectance and transmittance between the PC air waveguide with the collimator and the hollow core PBG fiber (Bragg waveguide) for a range of parameters. We consider fiber refractive indices in the range of $n_1=1.5$ to $n_1=1.8$ and fiber core diameters in the range of $D=1.1A$ to $D=2.5A$. Figure 9 shows the best coupling obtained with the collimator included. Although the fiber can capture 98% of the light exiting the waveguide (defined as the power transmitted into the fiber guided mode divided by the total power that exits PC waveguide) there is nearly 10% back reflection

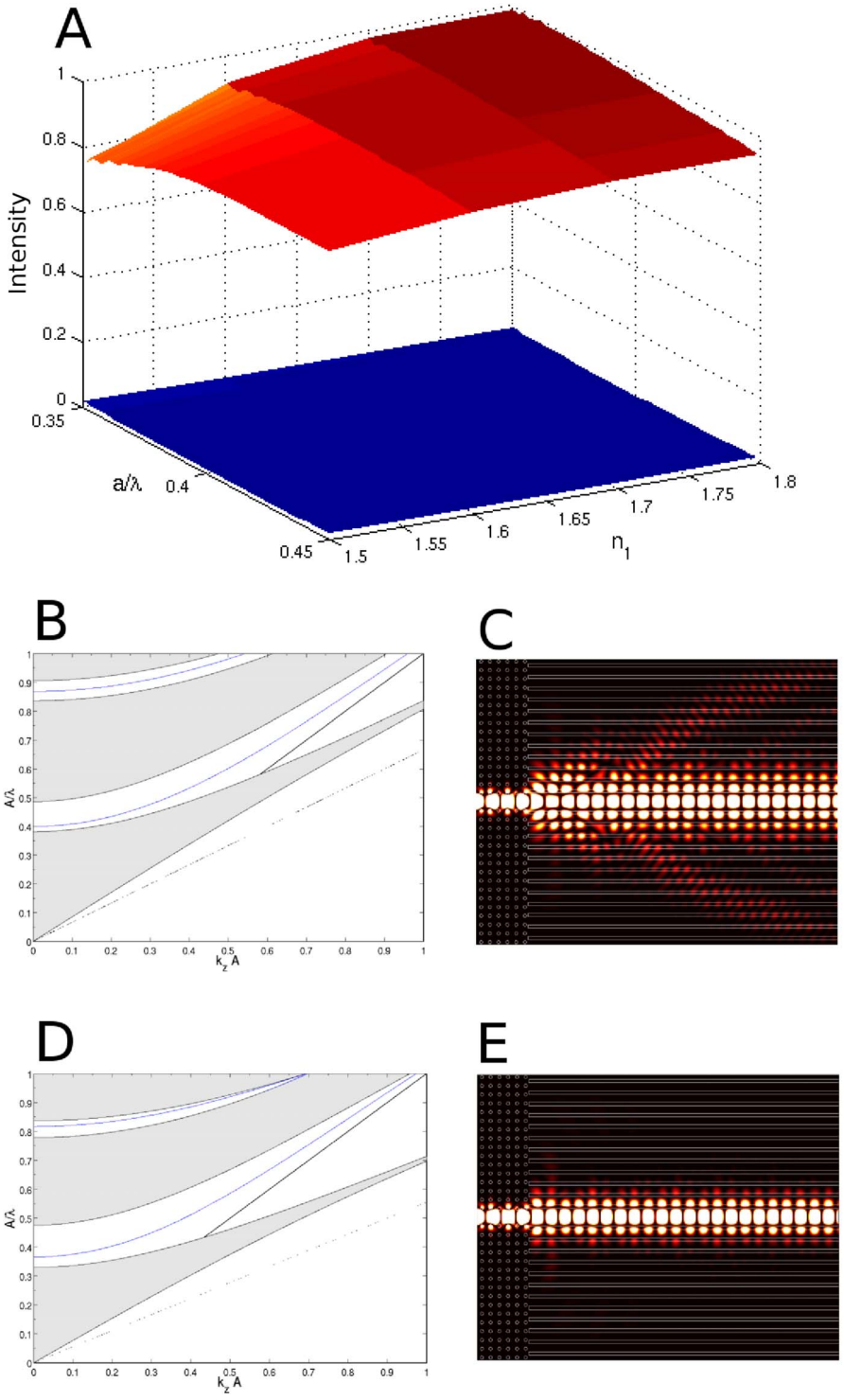

FIG. 8. (Color online) (a) The transmittance (upper surface) and reflectance (lower surface) as a function of both frequency a/λ and index of refraction n_1 for light coupling from a PBG air waveguide to a hollow core PBG fiber (see Fig. 6). Here $A/a=1.3$, $D=1.6A$, $d_1=0.3A$, $d_2=0.7A$, and $n_2=1.0$. The PBG waveguide parameters are $\epsilon_{rod}=11.9$, $\epsilon_{background}=1.0$, and $r=0.15a$. (b) The dispersion relation of the hollow core fiber even modes (as in Fig. 5, there is a lower-order mode and a higher-order mode) with $n_1=1.5$ and $D=1.6A$. The horizontal axis is (k_zA) and the vertical axis is a/λ. (c) A snapshot of the steady-state electric field intensity at $a/\lambda=0.4$ for coupling between the PBG air waveguide and the hollow core fiber with $n_1=1.5$. Weak coupling to the fiber cladding bands causes loss. (d) The even-mode dispersion relation for a hollow core fiber with $n_1=1.8$, with the guided modes as in (b). (e) A snapshot of the steady-state electric field intensity at $a/\lambda=0.4$ for coupling between the waveguides with $n_1=1.8$. Coupling to the fiber cladding modes is now diminished.

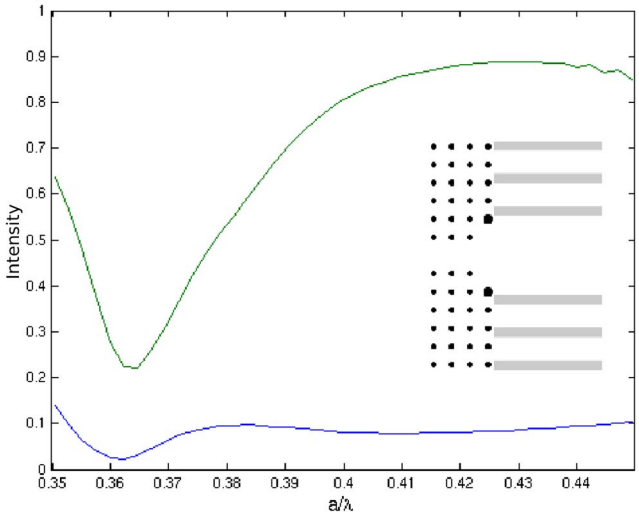

FIG. 9. (Color online) Transmittance (upper curve) and reflectance (lower curve) for coupling from the PBG air waveguide with exit port beam collimator to a hollow core PBG fiber. The structure is shown in the inset. The PC structural parameters are $r_{exit}=0.275a$, $\epsilon_{rod}=11.9$, $\epsilon_{background}=1.0$, and $r=0.15a$, where a is the PC lattice constant. The Bragg waveguide has $d_1=0.3A$, $d_2=0.7A$, $n_1=1.8$, $n_2=1.0$, $D=2.4A$, and $A/a=1.8$. The beam collimator offers little advantage for coupling to an optimally designed hollow core PBG fiber. Roughly 10% back reflection is present even well above the collimator resonance frequency.

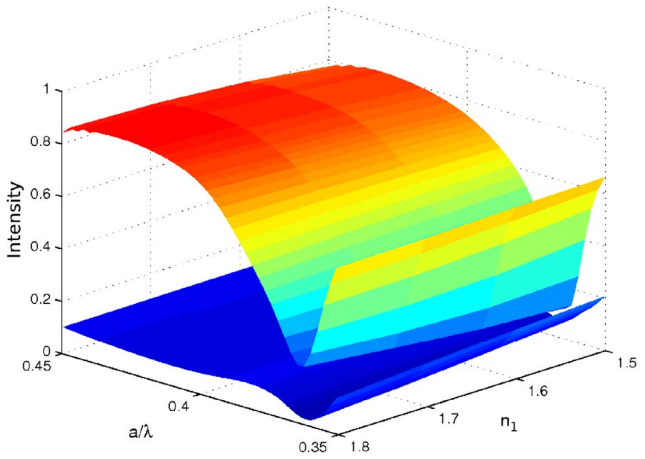

FIG. 10. (Color online) The transmittance (upper surface) and reflectance (lower surface) from PBG air waveguides to PBG hollow core fibers as a function of both frequency a/λ and index of refraction n_1, when the collimator is included (see Fig. 9). The hollow core fiber parameters are $D=2.4A$, $A/a=1.8$, $n_2=1.0$, and $d_1=0.3A$. The PC structural parameters are $r_{exit}=0.275a$, $\epsilon_{rod}=11.9$, $\epsilon_{background}=1.0$, and $r=0.15a$ where a is the PC lattice constant. The collimator offers slightly enhanced robustness of coupling as a function of n_1, at the expense of roughly 10% back reflection even well above the collimator resonance frequency.

into the PC over the frequency range of interest. This back-reflection problem appears to be a general feature of "beaming" into a hollow core fiber. In order to overcome this problem it is preferable (as shown is Sec. IV) to utilize a small-mode-area PBG fiber with a small solid core.

Notwithstanding this undesirable back reflection, the collimator offers the possibility of slightly more robust coupling to hollow fibers with lower values of cladding refractive index n_1. We calculate the portion of the light exiting the waveguide that is captured by the fiber with $n_1=1.5$. With the collimator, we find that 90% of the light exiting the PC waveguide is captured by the fiber in the best case, compared to 89% without the collimator. When the optimized fiber is used, the collimator does not reduce the losses to the cladding modes. Figure 10 shows the transmittance and reflectance as a function of a/λ and n_1. The highest transmittance occurs at $n_1=1.8$, but the sensitivity of this transmittance to n_1 is decreased by incorporating the collimator. With the collimator, the peak transmittance is only 7% lower for the $n_1=1.5$ fiber than for the best case $n_1=1.8$ waveguide. Without the collimator, the transmittance falls 11% from $n_1=1.8$ to $n_1=1.5$. When we vary the fiber core diameter D, the results are similar, both with and without the collimator: the transmittance remains insensitive to D over a broad range of fiber core diameters.

In summary, efficient and robust coupling is possible between an unmodified PC air waveguide and a hollow core PBG fiber. If the fiber cladding modes are properly engineered, the coupling efficiency is relatively insensitive to the fiber core diameter. The inclusion of a beam collimator at the PC air-waveguide exit port offers the possibility of slightly more robust coupling in the cladding refractive index degree of freedom at the expense of nearly 10% back reflection into the PC microchip. As a result, the most effective coupling from a PC air waveguide to a hollow core PBG fiber is obtained by simple butt coupling with no modification of the PC microchip exit port. For a silicon based ($\epsilon=11.9$) PC, the optimum hollow core fiber cladding refractive index is about $n_1=1.8$. In this case, 94% coupling efficiency (with a peak efficiency of 98%) is available over a bandwidth of 25% of the central frequency and the back reflection is typically less than 2%. In the next section, we demonstrate that the beam collimator can play a more essential role when light from the PC is coupled to a fiber with a small-mode-area solid core. In this case, we demonstrate even more efficient coupling (over 98% coupling throughout a bandwidth of nearly 10% of the central frequency).

IV. PBG CHIP TO SMALL-MODE-AREA PC-FIBER COUPLING

A. Small-mode-area PC fibers: 2D slab waveguide model

An alternative to the hollow core PBG fiber is the "small-mode-area" PC fiber [48]. This fiber has a small silica core ($\approx 1\ \mu m^2$ cross section) supported by a thin network of silica veins in air. In this case, the light that would normally be guided in the large air core of a PBG fiber is further concentrated into a subwavelength scale solid silica core. The two-dimensional analog of a small-mode-area solid-core fiber is a dielectric slab surrounded by air (the thin network of silica veins connecting the solid core to the outer cladding is neglected in our 2D model). Here we choose the dielectric

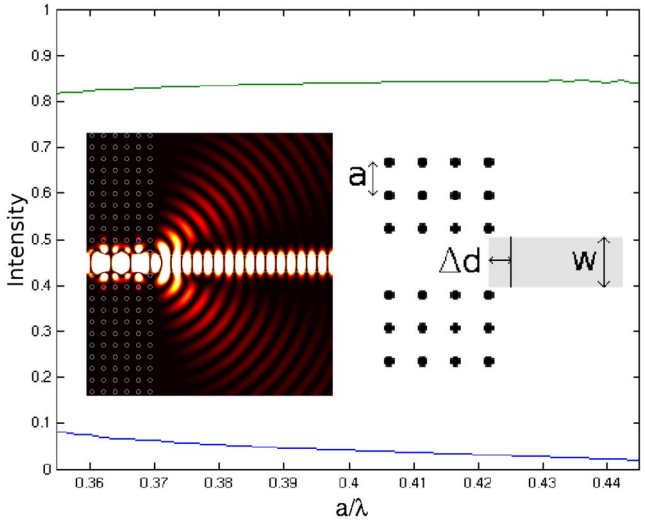

FIG. 11. (Color online) Transmittance (upper curve) and reflectance (lower curve) for light exiting an unmodified PBG air waveguide and coupling into a small-mode-area, solid-core photonic crystal fiber. In our slab waveguide model, the thin spokes connecting the solid core to the outer cladding are neglected [see Fig. 1(e)]. The PC parameters are $\epsilon_{rod}=11.9$, $\epsilon_{background}=1.0$, and $r=0.15a$ where a is the PC lattice constant and the slab parameters are $\Delta d=-0.5a$, $w=1.5a$, and $\epsilon_{slab}=2.25$. The left inset shows a snapshot of the electric field intensity near waveguide junction at $a/\lambda=0.4$. In the absence of beam collimation, there is significant loss due to diffraction.

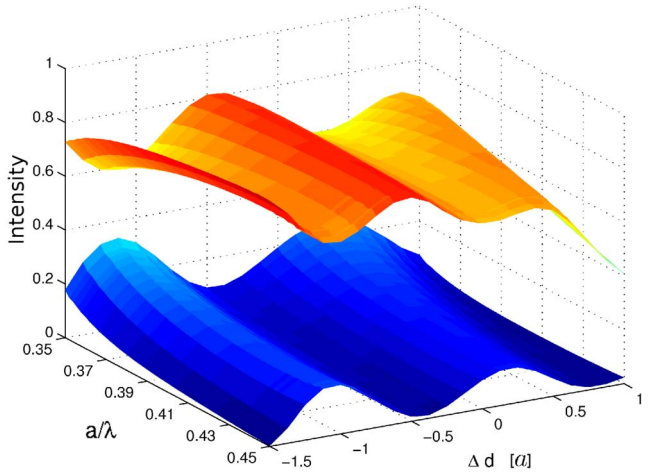

FIG. 12. (Color online) The transmittance (upper surface) and reflectance (lower surface) of the PBG air waveguide to small-mode-area, solid-core fiber junction (see Fig. 11) as a function of both frequency a/λ and fiber displacement Δd (in units of a). The fiber has a core width $w=1.5a$ and a core dielectric constant $\epsilon_{slab}=2.25$. The PBG air-waveguide parameters are $\epsilon_{rod}=11.9$, $\epsilon_{background}=1.0$, and $r=0.15a$ where a is the PC lattice constant. The oscillations in coupling as a function of Δd indicate wave interference between light reflected at the PBG surface and light reflected by the end of the fiber.

constant of the core $\epsilon_{core}=2.25$ and the immediate surrounding to be $\epsilon_{clad}=1.0$. We consider only even modes that have the same polarization as the PC waveguide. The odd modes and TE modes of the fiber do not couple with the even TM PC waveguide mode. We also restrict the slab width, w, so that only a single even mode is supported in the frequency range of interest. The cutoff frequency of the second even mode is obtained by solving Maxwell's equations. For a cutoff wavelength λ_c, the slab width (solid core diameter) must satisfy the inequality $w<\lambda_c(\epsilon_{core}-\epsilon_{clad})^{-1/2}$. We choose $a/\lambda=0.445$ (where a is the PC lattice constant) to be the cutoff frequency of the second-order even mode, limiting the slab width $w<2.01a$.

B. PC air waveguide to solid core fiber coupling

Here we consider coupling between the unmodified PC waveguide and the small-mode-area PC fiber slab waveguide. The PC waveguide is the same as that described in Sec. II. In the slab waveguide we hold the dielectric constants fixed ($\epsilon_{slab}=2.25$, $\epsilon_{cladding}=1.0$) and vary both the slab width w from $w=0.5a$ to $2.0a$ in $0.5a$ steps and the slab termination position Δd from $\Delta d=-1.5a$ to $1.0a$ in $0.125a$ steps [as measured from the hypothetical surface of the PC, $0.5a$ beyond the centers of the last row of rods (see Fig. 11)]. A Gaussian pulse with bandwidth that covers the PC waveguide bandwidth is excited in the PC waveguide. Then the reflection (transmission) spectra are determined by measuring the Fourier-transformed Poynting vector through a line $50a$ before (after) the PC waveguide-to-fiber junction. As discussed in Sec. III B, since we are coupling between two single-mode (even parity) waveguides, the transmission and reflection spectra are independent of the incidence direction. This was verified numerically using the finite difference time domain method.

Figure 11 shows the reflectance and transmittance spectra for the optimum structure within the structural parameter space. The transmittance ranges between 82% to 84.5% for the entire bandwidth. The reflectance varies between 8% and 2%. The left inset of Fig. 11 shows a snapshot of the steady-state electric field intensity at frequency $a/\lambda=0.4$. The transmittance at this frequency is 84% and the reflectance is 4%. The remaining fraction of the energy is lost symmetrically on either side of the slab waveguide. This is a remnant of the diffraction as light exits the subwavelength aperture of the PC waveguide. In the absence of an exit-port beam collimator, the small-mode-area fiber is not able to capture all of the light that exits the photonic crystal microchip.

The slab waveguide (solid core fiber) mode profile does not change drastically as the slab width changes. Consequently, the transmittance is not a strong function of fiber core width. The transmittance and reflectance change less than 2% when the slab width is changed from $w=0.5a$ to $w=2.0a$. However, changing the slab termination position, relative to the PC surface, does influence the coupling efficiency. This is depicted in Fig. 12. As Δd increases, the coupling efficiency decreases. This can be attributed to unmitigated diffraction as light exits the PC: The further the fiber is from the waveguide exit, the less light is coupled into the fiber core and the more light is lost in off-axis directions. As Δd is varied, we observe that the reflectance oscillates

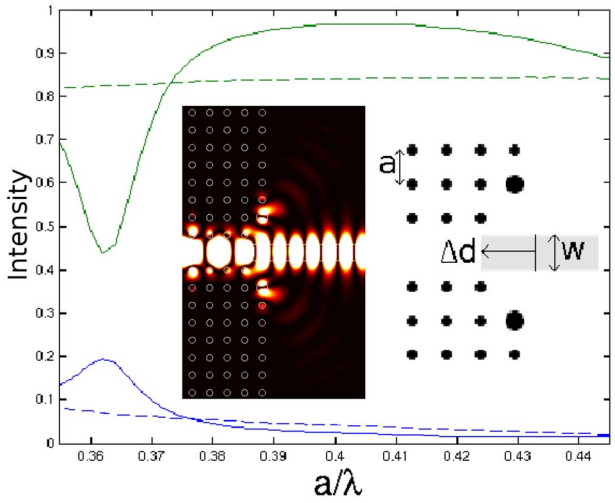

FIG. 13. (Color online) Reflectance (lower solid curve) and transmittance (upper solid curve) between the PBG air waveguide and a small-mode-area solid core fiber, including the beam collimator at the microchip waveguide exit port. The PBG structure has $\epsilon_{rod}=11.9$, $\epsilon_{background}=1.0$, $r=0.15a$, and $r_{exit}=0.275a$, where a is the PC lattice constant. The fiber parameters are $\epsilon_{slab}=2.25$, $w=1.0a$, and $\Delta d=-1.5a$. For comparison, the upper and lower dashed lines show the optimum transmission and reflection when the beam collimator is not included (i.e., the result shown in Fig. 11). The left inset shows a snapshot of the steady-state electric field intensity at $a/\lambda=0.4$. Here, the diffractive loss in the off-axis direction is negligible. The collimator is effective in reducing the off-axis diffraction seen in Fig. 11.

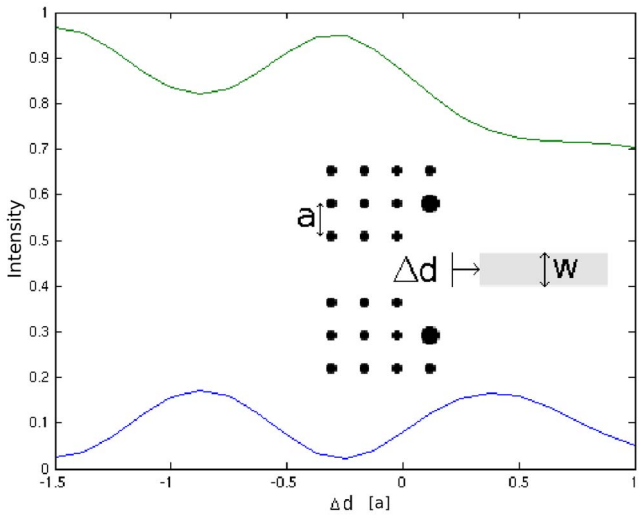

FIG. 14. (Color online) The transmittance (upper curve) and reflectance (lower curve) for light coupling from the PBG air waveguide to a small-mode-area, solid core fiber as a function of fiber core positioning Δd at fixed frequency $a/\lambda=0.4$ and fixed fiber core width $w=1.0a$. Δd is measured positive to the right of a line that ends $0.5a$ from the centers of the last row of rods. The PBG structure has $\epsilon_{rod}=11.9$, $\epsilon_{background}=1.0$, $r=0.15a$, and collimator rods with radius $r_{exit}=0.275a$, where a is the PC lattice constant. The fiber core dielectric constant is $\epsilon_{slab}=2.25$.

approximately 20% up and down. This reflectance oscillation is a consequence of wave interference between the two sources of back reflection. One source is the PC waveguide exit which remains fixed. The second (variable) source is the fiber core (slab waveguide) termination plane. The two reflected waves from these sources oscillate in and out of phase depending on the relative position of the fiber and the PC surface causing interference in the total reflectance. This effect was not present when coupling between PC waveguide and the hollow core fiber because of the negligible amplitude of the reflected wave from the hollow core fiber.

C. Collimated coupling to small-mode-area fiber

The exit-port collimator, depicted in Fig. 4, eliminates the light leaving the PBG microchip in the off-axis directions. Here we study the utility of this collimator on coupling efficiency to the small-mode-area fiber (slab waveguide). We replace the unmodified PC structure in Fig. 11 with the collimator structure shown in Fig. 4. The fiber (slab) parameters are varied from $w=0.5a$ to $2.0a$ in $0.5a$ steps and $\Delta d=-1.5a$ to $1.0a$ in $0.125a$ steps in search of the optimum coupling. Figure 13 shows the coupling efficiency for the optimum structure within the parameter space. For this particular structure, the back reflection drops below 5% at $a/\lambda=0.38$ and levels off at just below 2% by $a/\lambda=0.4$. The transmittance peaks at nearly 97%, and is higher than 94% between $a/\lambda=0.38$ and 0.43. The sum of the transmittance and reflectance with collimator is higher than without collimator, suggesting that the diffractive losses are reduced in this improved architecture. The left inset in Fig. 13 depicts a snapshot of the steady-state electric field intensity at $a/\lambda=0.4$, showing negligible off-normal diffraction due to the collimation effect.

The solid fiber core lowers the reflectance for specific positions, Δd, relative to when the collimator is beaming to free space. Figure 14 shows the reflectance and transmittance for the structure shown in Fig. 13 at frequency $a/\lambda=0.4$, for different slab termination positions. The oscillation in reflectance and transmittance spectra, as Δd varies, is due to interference between the two sources of back reflection as in the case of Fig. 12. This sensitivity of coupling efficiency to precise positioning of the fiber may be problematic in certain practical applications. The next two sections demonstrate the efficacy of a nonadiabatic taper in the solid core fiber in reducing unwanted reflectance back into the PC waveguide.

D. Coupling to a tapered small-mode-area fiber

In this section we introduce a nonadiabatic taper at the end of the small-mode-area fiber core (see structure in Fig. 15) in order to reduce back reflection at the chip to fiber junction. We calculate the reflectance and transmittance for various fiber core (slab) widths ($w=0.5a$ to $2.0a$ in $0.5a$ steps) and taper lengths ($\Delta T=0.0a$ to $3.5a$ in $0.25a$ steps).

Figure 15 shows the coupling efficiency for the tapered slab with the highest transmittance. The reflectance is less than 1% between $a/\lambda=0.37$ and $a/\lambda=0.43$. This is clearly less than in the absence of a taper. The transmittance peaks at

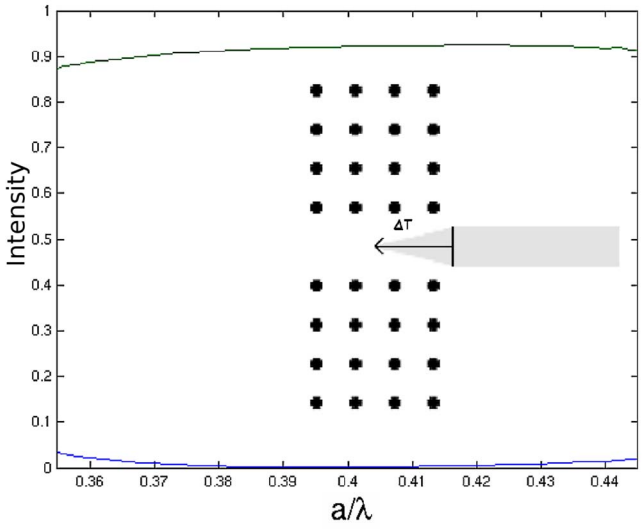

FIG. 15. (Color online) The transmittance (upper curve) and reflectance (lower curve) for light coupling between a PBG air waveguide with no collimation architecture and a small-mode-area, solid-core fiber with a nonadiabatic taper. Here, the fiber core width is $w=1.0a$, the taper length is $\Delta T=2a$, and $\epsilon_{slab}=2.25$. The PBG structure has $\epsilon_{rod}=11.9$, $\epsilon_{background}=1.0$, and $r=0.15a$ where a is the PC lattice constant. In comparison to Fig. 11, the fiber core taper is highly effective in reducing back reflection at the junction. Beam collimation (see Fig. 17) is still required to eliminate off-axis diffractive loss.

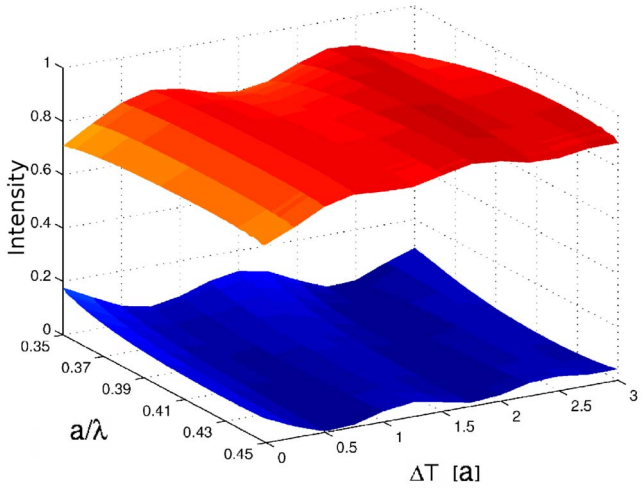

FIG. 16. (Color online) The transmittance (upper surface) and reflectance (lower surface) for light coupling from a PBG air waveguide to the tapered small-mode-area solid core fiber (see Fig. 15) as a function of both taper length ΔT (in units of a) and normalized frequency a/λ, for a fixed fiber core width $w=1.0a$. The fiber core dielectric constant is $\epsilon_{slab}=2.25$ and the PBG parameters are $\epsilon_{rod}=11.9$, $\epsilon_{background}=1.0$, and $r=0.15a$ where a is the PC lattice constant.

92% and stays above 90% over a frequency range of $a/\lambda=0.37$ to 0.445. In the absence of a collimation architecture, there are losses of more than 8% due to diffraction in the off-normal direction. However, in the nontapered fiber geometry, 13.5% of the light exiting the PC waveguide is lost through diffraction. This suggests that the taper, in addition to eliminating reflection, is helping to convert the PC waveguide mode to the fiber core mode.

Figure 16 shows the transmittance and reflectance as a function of frequency a/λ and ΔT for $w=1.0a$. We see that the reflectance spectrum oscillates as a function of ΔT, suggesting that a path-length dependent phase change of the reflected wave from the slab is occurring, as in the nontapered case. The amplitude of these oscillations is not as high as in the nontapered case. Figure 16 also shows that for a given slab taper ΔT the frequency response is relatively flat, with variations in the reflectance or transmittance spectra of only about 7% from lowest to highest frequency.

E. Collimated coupling to a tapered small-mode-area fiber

Finally, we demonstrate that the collimator architecture, introduced in Fig. 4, improves the coupling efficiency of the previous design by minimizing diffractive losses in the off-normal direction without compromising the elimination of reflection. We calculate the transmittance and reflectance for the PC structure including the collimator, and vary the slab (fiber core) parameters as in the previous section.

Figure 17 shows reflectance and transmittance for the PC air waveguide to fiber interface, including the collimator. The reflectance is nearly eliminated, being less than 1% between $a/\lambda=0.38$ and 0.445. This cancellation suggests that the amplitude of the reflected wave from the two reflection sources (the collimator and fiber core) are more closely matched. The collimator also nearly eliminates off-normal diffractive losses and the resulting transmittance is better than 90% between $a/\lambda=0.378$ and 0.45, or 17% percent of the center frequency. The transmittance is more than 98% over a bandwidth of 9% of the center frequency. At present-day telecommunications frequencies (1.5 μm), this covers a bandwidth of 135 nm. The taper length is chosen to minimize reflectance and optimize conversion of the PC waveguide mode to the fiber core mode.

Figure 18 shows the transmittance and reflectance as a function of a/λ and ΔT for a slab width of $w=1.5a$. The reflectance oscillates as the taper length changes, indicating a variation in phase of the reflected wave from the fiber core due to the change in path length. As the taper length increases, the reflectance is reduced, and the transmittance improves at higher frequencies. The collimator reduces the off-axis diffractive losses, and the taper helps to convert the PC waveguide mode to the slab waveguide mode.

In summary, the PC to fiber coupling without the collimator can be 84.5% efficient with proper choice of fiber core parameters, but can be improved to 92% when a small taper is introduced in the solid core of the small-mode-area fiber. The results are relatively insensitive to the frequency of the light and the fiber core width, but are sensitive to the placement of the fiber and the taper length. When the collimator is also included, the coupling efficiency increases to 97% without a taper and can exceed 98% over a bandwidth of 9% of the center frequency when fiber core is suitably tapered. The collimator reduces the off-axis diffractive losses. The taper

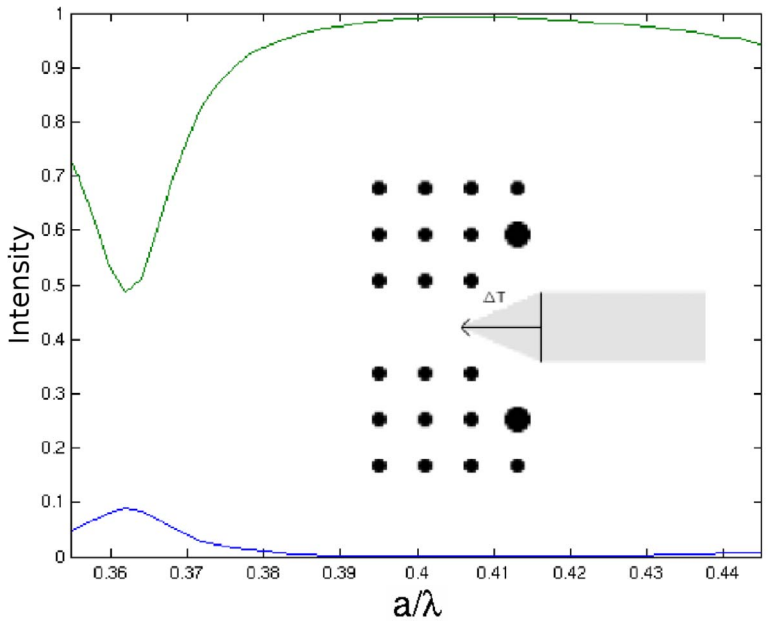

FIG. 17. (Color online) The transmittance (upper curve) and reflectance (lower curve) for light coupling from a PBG air waveguide (with the beam collimator) to a tapered small-mode-area solid core fiber. The PBG parameters are $\epsilon_{rod}=11.9$, $\epsilon_{background}=1.0$, with collimator rod radius $r_{exit}=0.275a$ and bulk rod radius $r=0.15a$, where a is the PC lattice constant. The fiber core parameters are $\epsilon_{slab}=2.25$, $w=1.5a$, and $\Delta T=1.75a$. Here over 98% coupling efficiency is achieved over a range of 9% of the optimum wavelength defined by $a/\lambda=0.41$. If this optimum wavelength is chosen to be 1.5 μm, then this near perfect coupling is maintained over a bandwidth of 135 nm.

plays two roles: to reduce back reflectance by destructive interference with reflectance from the PC waveguide termination and to facilitate conversion of the PC waveguide mode to the fiber core mode.

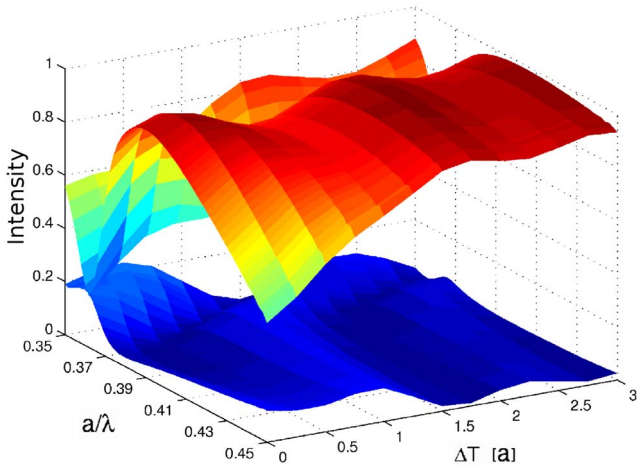

FIG. 18. (Color online) The transmittance (upper surface) and reflectance (lower surface) for light coupling from the PBG air waveguide (with the beam collimator) to the tapered small-mode-area solid-core fiber (see Fig. 17) as a function of both taper length ΔT and normalized frequency a/λ, for a fixed fiber core width $w=1.5a$. The PBG chip has $\epsilon_{rod}=11.9$, $\epsilon_{background}=1.0$, $r_{exit}=0.275a$, and $r=0.15a$, where a is the PC lattice constant. The dielectric constant of the fiber core is $\epsilon_{slab}=2.25$. The taper improves the high-transmission bandwidth.

V. CONCLUSIONS

A crucial requirement for deployment of PBG chips in optical telecommunication networks is the ability to couple light, without loss, to and from long-haul optical fibers. We have shown, using a 2D model, that by combining beam collimation at the PBG chip exit port with the additional design freedom of microstructured PBG fibers, large bandwidth, low-loss coupling is possible. We find that a hollow core fiber end coupled to a PBG air waveguide allows 94% coupling efficiency. The 25% working bandwidth of this design translates to a bandwidth of 375 nm when operating at 1.5 μm. Alternatively, coupling small-mode-area PBG fibers to PBG microchips leads to the best available coupling over a bandwidth of 135 nm. The inclusion of the large-bandwidth beam collimator nearly eliminates diffractive losses, and nonadiabatically tapering the fiber can minimize the reflection at the junction. Combining these two design facets, we find coupling between small-mode-area fibers and PBG air waveguides with efficiencies of 98% over a working bandwidth of 9% of the central wavelength (135 nm at a working wavelength of 1.5 μm.). These 2D design paradigms suggest similar high efficiency coupling may be possible in realistic 3D fiber to chip junctions. 3D systems introduce some issues not present in 2D. The electromagnetic field polarization degree of freedom must be taken into account. Typical fibers with roughly circular symmetry have TE-TM hybrid modes where the polarization is closer to circular than TM- or TE- type. In contrast, the 3D PBG heterostructure [9,10] waveguide has a TM-like mode profile. The dimensional asymmetry of the heterostructure waveguide

(with a width to height ratio of roughly 2.5:1) will likely require an asymmetrical small-mode-area solid core fiber for efficient fiber to chip coupling. After interfacing with PBG microchips, the specialty PBG fibers proposed here may then be adiabatically tapered over centimeter scales to merge into more conventional long-haul optical fibers. This would complete the connection between long haul optical fibers and PBG microchip architectures.

ACKNOWLEDGMENTS

We are grateful to Dr. Alongkarn Chutinan for helpful discussions. This work was supported in part by the Natural Sciences and Engineering Research Council of Canada, the Canadian Institute of Advanced Research, and the Ontario Premier's Platinum Research Fund.

[1] S. John, Phys. Rev. Lett. **58**, 2486 (1987).
[2] E. Yablonovitch, Phys. Rev. Lett. **58**, 2059 (1987).
[3] S. John, Phys. Rev. Lett. **53**, 2169 (1984).
[4] J. D. Joannopoulos, R. D. Mead, and J. N. Winn, *Photonic Crystals: Molding the Flow of Light* (Princeton University Press, Princeton, NJ, 1995).
[5] S. Fan, P. R. Villeneuve, J. D. Joannopoulos, and H. A. Haus, Phys. Rev. Lett. **80**, 960 (1998).
[6] A. Mekis, J. C. Chen, I. Kurland, S. Fan, P. R. Villeneuve, and J. D. Joannopoulos, Phys. Rev. Lett. **77**, 3787 (1996).
[7] A. Chutinan, S. John, and O. Toader, Phys. Rev. Lett. **90**, 123901 (2003).
[8] A. Chutinan and S. John, Phys. Rev. E **71**, 026605 (2005).
[9] A. Chutinan and S. John, Opt. Express **14**, 1266 (2006).
[10] M. Deubel, M. Wegener, S. Linden, G. V. Freymann, and S. John, Opt. Lett. **31**, 805 (2006).
[11] Y. Xu, R. K. Lee, and A. Yariv, Opt. Lett. **25**, 755 (2000).
[12] A. Mekis and J. D. Joannopoulos, J. Lightwave Technol. **19**, 861 (2001).
[13] S. G. Johnson, P. Bienstman, M. A. Skorobogaitiy, M. Ibanescu, E. Lidorikis, and J. D. Joannopoulos, Phys. Rev. E **66**, 066608 (2002).
[14] P. Bienstman, S. Assefa, S. G. Johnson, J. D. Joannopoulos, G. S. Petrich, and L. A. Kolodziejski, J. Opt. Soc. Am. B **20**, 1817 (2003).
[15] E. H. Khoo, A. Q. Liu, and J. H. Wu, Opt. Express **13**, 7748 (2005).
[16] R. Stoffer, H. J. W. M. Hoekstra, R. M. D. Ridder, E. V. Groesen, and F. P. H. V. Beckum, Opt. Quantum Electron. **32**, 947 (2000).
[17] A. Adibi, Y. Xu, R. K. Lee, A. Yariv, and A. Scherer, Phys. Rev. B **64**, 033308 (2001).
[18] M. Qui, K. Azizi, A. Karlsson, M. Swillo, and B. Jaskorzynska, Phys. Rev. B **64**, 155113 (2001).
[19] E. Miyai, M. Okano, M. Mochizuki, and S. Noda, Appl. Phys. Lett. **81**, 3729 (2002).
[20] M. Badieirostami, B. Momeni, M. Soltani, A. Adibi, Y. Xu, and R. K. Lee, Opt. Express **12**, 4781 (2004).
[21] M. Palamaru and P. Lalanne, Appl. Phys. Lett. **78**, 1466 (2001).
[22] P. Lalanne and A. Talneau, Opt. Express **10**, 354 (2002).
[23] A. Talneau, P. Lalanne, M. Agio, and C. M. Soukoulis, Opt. Lett. **27**, 1522 (2002).
[24] L. Rosa, S. Selleri, and F. Poli, J. Lightwave Technol. **23**, 2740 (2005).
[25] T. Tamir and S. T. Peng, Appl. Phys. (Berlin) **14**, 235 (1977).
[26] N. Eriksson, M. Hadberg, and A. Larsson, IEEE Photonics Technol. Lett. **7**, 1394 (1995).
[27] N. Eriksson, M. Hadberg, and A. Larsson, IEEE J. Quantum Electron. **32**, 1038 (1996).
[28] T. W. Ang, G. T. Reed, A. Vonsovici, A. G. R. Evans, P. R. Routley, and M. R. Josey, IEEE Photonics Technol. Lett. **12**, 59 (2000).
[29] D. Taillaert, W. Bogaerts, P. Bienstman, T. F. Krauss, I. Moerman, P. V. Daele, and R. Baets, in 27th European Conference on Optical Communication 2001 ECOC'01 (unpublished), Vol. 6, pp. 30–31.
[30] D. Taillaert, W. Bogaerts, P. Bienstman, T. F. Krauss, P. V. Daele, I. Moerman, S. Verstuyft, K. D. Mesel, and R. Baets, IEEE J. Quantum Electron. **38**, 949 (2002).
[31] D. Taillaert, P. Bienstman, and R. Baets, Opt. Lett. **29**, 2749 (2004).
[32] P. Sanchis, J. Marti, J. Blasco, A. Martinez, and A. Garcia, Opt. Express **10**, 1391 (2002).
[33] P. Sanchis, J. Marti, A. Garcia, A. Martinez, and J. Blasco, Electron. Lett. **38**, 961 (2002).
[34] P. Sanchis, A. Garcia, J. Marti, W. Bogaerts, P. Dumon, D. Taillairt, R. Baets, V. Wiaux, J. Wouters, and S. Beckx, IEEE Photonics Technol. Lett. **16**, 2272 (2004).
[35] A. Hakansson, P. Sachis, J. Sanches-Dehesa, and J. Marti, J. Lightwave Technol. **23**, 3881 (2005).
[36] J. Jiang, J. Cai, G. P. Nordin, and L. Li, Opt. Lett. **28**, 2381 (2003).
[37] P. E. Barclay, K. Srinivasan, and O. Painter, in PECS-IV: International Workshop on Photonic and Electromagnetic Crystal Structures (University of California, Los Angles, 2002), p. 38
[38] P. E. Barclay, K. Srinivasan, M. Borselli, and O. Painter, Electron. Lett. **39**, 842 (2003).
[39] P. E. Barclay, K. Srinivasan, and O. Painter, J. Opt. Soc. Am. B **20**, 2274 (2003).
[40] P. E. Barclay, K. Srinivasan, M. Borselli, and O. Painter, Opt. Lett. **29**, 697 (2004).
[41] P. E. Barclay, K. Srinivasan, M. Borselli, and O. Painter, Appl. Phys. Lett. **85**, 4 (2004).
[42] W. Kuang, C. Kim, A. Stapleton, and J. D. O'Brien, Opt. Lett. **27**, 1604 (2002).
[43] C. Grillet, C. Smith, D. Freeman, S. Madden, B. Luther-Davies, E. C. Magi, D. J. Moss, and B. J. Eggleton, Opt. Express **14**, 1070 (2006).
[44] A. Ferrando, E. Silvestre, J. J. Miret, and P. Andres, Opt. Lett. **25**, 790 (2000).
[45] J. C. Knight, J. Arriaga, T. A. Birks, A. Ortigosa-Blanch, W. J. Wadsworth, and P. S. J. Russell, IEEE Photonics Technol. Lett. **12**, 807 (2000).

[46] T. A. Birks, J. C. Knight, and P. S. J. Russell, Opt. Lett. **22**, 961 (1997).
[47] R. F. Cregan, B. J. Mangan, J. C. Knight, T. A. Birks, P. S. J. Russell, P. J. Roberts, and D. C. Allan, Science **285**, 1537 (1999).
[48] Y. K. Lize, E. C. Magi, V. G. Taeed, J. A. Bolger, P. Steinvurzel, and B. J. Eggleton, Opt. Express **12**, 3209 (2004).
[49] A. Ortigosa-Blanch, J. C. Knight, W. J. Wadsworth, J. Arriaga, B. J. Mangan, T. A. Birks, and P. S. J. Russell, Opt. Lett. **25**, 1325 (2000).
[50] J. Broeng, S. E. Barkou, and A. Bjarklev, Opt. Fiber Commun. **3**, 101 (2000).
[51] J. D. Jackson, *Classical Electrodynamics*, 3rd ed. (Wiley, New York, 1999).
[52] R. D. Meade, K. D. Brommer, A. M. Rappe, and J. D. Joannopoulos, Phys. Rev. B **44**, 10961 (1991).
[53] P. Kramper, M. Agio, C. M. Soukoulis, A. Birner, F. Muller, R. B. Wehrspohn, U. Gosele, and V. Sandoghdar, Phys. Rev. Lett. **92**, 113903 (2004).
[54] S. K. Morrison and Y. S. Kivshar, Appl. Phys. Lett. **86**, 081110 (2005).
[55] E. Moreno, F. J. Garcia-Vidal, and L. Martin-Moreno, Phys. Rev. B **69**, 121402 (2004).
[56] I. Bulu, H. Caglayan, and E. Ozbay, Opt. Lett. **30**, 3078 (2005).
[57] S. K. Morrison and Y. S. Kivshar, Appl. Phys. Lett. **86**, 081110 (2005).
[58] W. R. Frei, D. A. Tortorelli, and H. T. Johnson, Appl. Phys. Lett. **86**, 111114 (2005).
[59] W. R. Frei, D. A. Tortorelli, and H. T. Johnson, Opt. Lett. **32**, 77 (2007).
[60] A. Taflove and S. Hagness, *Computational electrodynamics: The finite difference time-domain method* (Artech House, Norwood, MA, 2005).